

MoS₂ Liquid Cell Electron Microscopy Through Clean and Fast Polymer-Free MoS₂ Transfer

*Jiwoong Yang,^{†,◊} Moon Kee Choi,^{‡,§,◊} Yuewen Sheng,^{||} Jaebong Jung,[⊥] Karen Bustillo,[#]
Seung-Wuk Lee,^{‡,§} Peter Ercius,[#] Ji Hoon Kim,[⊥] Jamie H. Warner,^{||} Emory M. Chan,[#] and
Haimei Zheng^{†,▽,*}*

[†] Materials Sciences Division, Lawrence Berkeley National Laboratory, Berkeley, California
94720, United States

[‡] Department of Bioengineering and Tsinghua Berkeley Shenzhen Institute, University of
California, Berkeley, California 94720, United States

[§] Biological Systems and Engineering Division, Lawrence Berkeley National Laboratory,
Berkeley, California 94720, United States

^{||} Department of Materials, University of Oxford, 16 Parks Road, Oxford OX1 3PH, United
Kingdom

[⊥] School of Mechanical Engineering, Pusan National University, Busan 46269, Korea

[#] The Molecular Foundry, Lawrence Berkeley National Laboratory, Berkeley, California
94720, United States

[▽] Department of Materials Science and Engineering, University of California, Berkeley,
California 94720, United States

[◊] J. Yang and M. K. Choi contributed equally to this work.

*E-mail: hmzheng@lbl.gov

ABSTRACT

Two dimensional (2D) materials have found various applications. For example, graphene has been used as the electron transparent membrane for liquid cell transmission electron microscopy (TEM). Here, we report using MoS₂ 2D materials as the functional substrates as well as the membrane window for liquid cell TEM. The development of MoS₂ liquid cells is enabled by a facile and polymer-free MoS₂ transfer process. This provides the opportunity to investigate the formation of Pt nanocrystals on MoS₂ substrates. We find that Pt nanocrystals formed in MoS₂ liquid cells have the strong tendency to align their crystal lattice with that of MoS₂ (Pt {111} // MoS₂ {100}), suggesting the van der Waals epitaxial relationship between Pt nanocrystals and MoS₂. The development of MoS₂ liquid cells will allow the further study of liquid phenomena and nanomaterials formation on MoS₂ 2D films and the polymer-free MoS₂ transfer process will be applied to various studies.

KEYWORDS

MoS₂, liquid cell electron microscopy, polymer-free transfer, nanocrystal formation, heterostructures

Liquid cell transmission electron microscopy (TEM) allowing imaging through liquids with high spatial and temporal resolution have enabled the study of various dynamic phenomena in liquids, ranging from nanoscale crystallization¹⁻⁵ to transformation,⁶⁻¹⁰ self-assembly,¹¹⁻¹⁴ electrochemical,¹⁵⁻¹⁷ and biological process.^{18,19} The recent applications of 2D materials, such as graphene for the membrane window of liquid cells,²⁰⁻²⁷ has significantly enhanced the image contrast by reducing electron beam scatterings during imaging.²⁸ In deed, graphene has been utilized as an excellent membrane material for conventional TEM^{29,30} due to its high thermal/electrical conductivity,³¹ chemical inertness,³² impermeability for small molecules,³³ high mechanical strength and flexibility.³⁴ Currently, the applications of 2D materials for liquid cell TEM has mostly focused on graphene^{19-27,35-38} or graphene oxide³⁹ and their roles are limited to the encapsulating material or providing mechanical supports. Exploration of other 2D materials for liquid cell TEM will allow for investigation of the liquid phenomena taking place on different 2D materials.

Because of the synergetic effects between the 2D materials and the nanomaterials with various dimensionalities (0D, 1D, and 2D) being introduced, heterostructured 2D materials have emerged as an important class of materials offering unique properties.⁴⁰⁻⁴⁶ There have been tremendous efforts on the synthesis and characterization of a variety forms of the 2D heterostructures, among which heterostructures composed of MoS₂ with noble metal nanoparticles such as Pt and Pd have attracted a lot of attention due to their enhanced catalytic performance.⁴⁷⁻⁵¹ It has been known that the properties of the heterostructured 2D materials are highly sensitive to their atomic structures such as the relative crystal orientation of the constituent materials.^{52,53} An understanding and ultimately controlling of the noble metal nanoparticle formation on the 2D substrates is of key importance to fully exploit them for further applications. The previous studies have been conducted mostly by *ex situ* structure characterization or *in situ* TEM heating experiments under high vacuum.⁵⁴⁻⁵⁶

Development of an effective and reproducible transfer process is one of the prerequisites for applications of 2D materials into the well-designed format.^{57,58} They are usually grown on growing substrates by chemical vapor deposition (CVD) methods thus need to be transferred on target substrates for further usage.⁵⁹⁻⁶³ Conventionally, spin-casted polymer layers have been employed to protect 2D materials from mechanical damage during the transfer process.⁶⁴⁻⁶⁹ However, it is hard to completely remove them and the polymer residues may deteriorate their optical, electrical, electrochemical or mechanical properties.⁷⁰⁻⁷⁴ Especially, for liquid cell TEM, it can significantly interrupt the imaging and result in various side-reactions by interacting with liquid species under electron beam.^{35-38,75,76} The polymer-free transfer method has been developed for graphene⁷⁷⁻⁷⁹ since the substrate (Cu) can be easily etched in mild condition without introducing significant mechanical damage to graphene.^{19-27, 35-38,79} However, transition metal chalcogenides (such as, MoS₂, WS₂) are usually deposited on SiO₂/Si wafers⁸⁰⁻⁸⁴, which requires the harsh reaction conditions (hot alkaline solution or high energy ultrasonic processes) to remove the Si substrates can damage the 2D films. Thus, the development of polymer-free transfer for MoS₂ has been a daunting goal.

Here, we report the development of MoS₂ liquid cells through a fast and polymer-free transfer process for *in situ* TEM study of Pt nanocrystal growth on MoS₂. The selective etching of the interfacial SiO₂ layer between MoS₂ and Si wafer effectively reduces mechanical damage and results in high transfer yield. The mechanical stability of MoS₂ during the transfer process is supported by finite element analysis. The transferred MoS₂ in liquid cells are employed as functional substrate to investigate Pt nanocrystal formation on MoS₂ through *in situ* TEM. Our work suggests a facile and clean transfer method for MoS₂ and will help to facilitate fundamental understandings of liquid phenomena that occur on 2D materials.

The procedure of polymer-free MoS₂ transfer as the functional substrate for *in situ* liquid cell TEM is shown in Figure 1 (See Methods 1.1, 1.2, Figures S1 and S2 in the Supporting

Information (SI) for experimental details). Quantifoil carbon grids with the regular empty hole arrays (diameter: $\sim 1.2\ \mu\text{m}$ or $2\ \mu\text{m}$) are used as target substrates, which allows the applications and further characterization of the regions of free standing transferred-MoS₂ sheets. We directly attach the Quantifoil carbon TEM grids on MoS₂/SiO₂/Si without polymer protection layers and use HF to selectively etch the interfacial SiO₂ layers. The MoS₂ sheet is then transferred onto the TEM grids. Scanning electron microscopy (SEM) images of the MoS₂-transferred TEM grids show almost perfect coverage of the Quantifoil holes with MoS₂ (Figure 1b, Figures S3 and S4 in SI) regardless of window size (average transfer yields of $\sim 96\%$ and $\sim 91\%$ for the hole size of $\sim 1.2\ \mu\text{m}$ and $\sim 2\ \mu\text{m}$, respectively).

For comparison, we also carried out MoS₂ transfer with conventional method using KOH etching (See Method 1.2 in SI for experimental details). The gaseous byproducts (H₂) generated during KOH etching⁸⁰⁻⁸² can easily damage MoS₂ sheets. Therefore, the polymer layer is essential to protect MoS₂ sheets from damage during the conventional transfer process. With polymer protection, a high transfer yield ($\sim 95\%$) is achieved. However, the complete removal of polymer residues is challenging (Figure S5 in SI), which would be problematic for further applications in liquid cell TEM, due to the poor visibility and undesirable side-reactions induced by the polymer residues during imaging. Without polymer protection layer, only a small fraction of MoS₂ sheets can be transferred ($\sim 10\%$) and the most of them are perforated (Figure 1b and Figure S6 in SI).

Theoretical analysis based on Finite element method (FEM) simulation validates the high transfer yield of our polymer-free MoS₂ transfer process (See the Method 1.3 in SI for details). First, we test the role of target substrate against bending stress. Figure 1c shows the representative stress distribution over MoS₂ sheets during the etching process with/without the prelaminated target substrate. The maximum applied stress on the MoS₂ sheets attached with the carbon/gold layer is more than one order lower than that of freestanding MoS₂ sheets under

the same applied pressure. This implies that the target substrates can effectively act as a protecting layer. Second, FEM calculations estimate the mechanical impact of the bubble generation on MoS₂ sheets floating on the etching solution (Figure 1d and Figure S7 in SI). When bubbles are trapped under MoS₂ sheets, they can cause local stretching of the freestanding MoS₂ sheets. Especially at the edge of the bubbles, the local stress is significant regardless of the bubble size. This suggests that the vigorous bubble generation during the KOH etching process with the relatively long reaction time (tens of minutes) can break the MoS₂. In addition to the reduced bending and stretching stress, our selective etching reaction takes a very short reaction time (< ~1 sec), which is 1,000 times shorter than that of the conventional KOH etching (Figure S8 in SI). This also helps to minimize the chance of mechanical damages on MoS₂ during the etching process.

Figure 2a shows a representative low-resolution TEM image of the MoS₂-transferred Quantifoil TEM grid (see Method 1.5 in SI). High-resolution TEM images of the two different freestanding MoS₂ region reveal the clean surface with atomic structure of MoS₂ (Figure 2b,c). A fast Fourier transform (FFT) of the TEM image displays hexagonally arranged spots with ~0.27 nm spacings, corresponding to the MoS₂ {100} lattice planes (Figure 2d). A set of the spots corresponding to the MoS₂ {110} lattice planes (~0.17 nm) and higher order diffraction spots are also shown in the FFT pattern, which is attributed to the large high resolution TEM image with nearly perfect atomic arrangement. With the clean surface, atomic resolution TEM images of MoS₂ can be easily obtained without post-image processing or the advanced TEM such as aberration-correction or direct electron detection. TEM image obtained at the broken parts of MoS₂ confirms that the MoS₂ used in this study is 2–4 layers (Figure S9 in SI). Furthermore, our transfer process can be applied repeatably to produce multiple stacking of MoS₂. TEM images of stacked structures exhibit the Moiré patterns corresponding to the alignment of constituent MoS₂ layers (Figure S10 in SI).

We further characterize the MoS₂ sheets using Raman spectroscopy. **Figure 2e** shows the Raman spectra of MoS₂ before (i.e. MoS₂/SiO₂/Si) and after (i.e. MoS₂-transferred grids) the transfer process. Both spectra clearly exhibit the characteristic peaks of MoS₂ (E_{2g}^1 mode at $\sim 384\text{ cm}^{-1}$ and A_{1g} mode at $\sim 407\text{ cm}^{-1}$) without noticeable differences⁸⁵⁻⁸⁷. A slight stiffening of the A_{1g} mode can be attributed to the substrate effect.^{86,87} Since the Raman spectra of 2D materials are highly related to the atomic arrangement of the samples,⁸⁸ these experimental results confirm that the structure of the MoS₂ is well maintained during the transfer process.

The transferred MoS₂ sheets are used for the fabrication of TEM liquid cells and further study of Pt nanocrystal formation on MoS₂. The Pt nanocrystal growth solution can be successfully encapsulated between MoS₂- and graphene-transferred grids for TEM imaging (**Figure 3a and Method 1.4 in SI**). Low-resolution TEM images display that the liquid pockets resemble a pseudo-rectangular shape (**Figure 3b and Figure S11 in SI**). The length (the longer axis) and the width (the shorter axis) of the liquid pockets are in the range of several hundreds of nanometers and several tens of nanometers, respectively (**Figure 3c,d**). The aspect ratio (length/width) of the liquid pockets is large (3–8) as shown in the histogram in **Figure 12 in SI**. The formation of the anisotropic liquid pockets with pseudo-rectangular shape is very different from the previous studies using graphene liquid cells with the similar Pt growth solution, where the liquid pockets are highly irregular (**Figure S13 in SI**). It is worth mentioning that MoS₂ liquid cells fabricated by the conventional transfer process using polymer protection layers show significant carbon contamination under the electron beam exposure (**Figure S14 in SI**), which limits any reliable liquid TEM study.

We further analyze the 4k×4k high-resolution TEM images of the liquid pockets (**Figure 3e-l**) to determine the distribution of MoS₂ grains around the liquid pockets (**See the Method 1.5 in SI**). FFT patterns of the whole images exhibit the several sets of hexagonally arranged spots corresponding to the MoS₂ lattices (**Figure 3f,j**). The multiple sets of the spots with slight

misorientations suggests the co-existence of the different MoS₂ grains, which is common in the CVD-grown multilayer-2D materials. We perform inverse FFT with selective masking to figure out the position of each grain. The grain distribution is highlighted by the color mapping in the original TEM images in [Figure 3e,i](#) and the representative high-resolution inverse FFT images are displayed in [Figure 3g,h](#) and [Figure 3k,l](#). The additional high-resolution inverse FFT images acquired from the different part of grain are presented in [Figures S15 and S16 in SI](#). We find that the liquid pockets tend to form between the different grains of MoS₂. This is likely due to the different surface properties of the MoS₂ surface vs at the defect sites (grain boundaries). Other factors, such as membrane bulging,⁸⁹ which is also expected to be significant at grain boundaries because of its low mechanical strength, may also affect the liquid distribution.

The successful fabrication of MoS₂ liquid cells provides the opportunity to investigate Pt nanocrystal formation on the MoS₂ with *in situ* liquid cell TEM. The growth of Pt nanocrystals has been well studied using *in situ* liquid cell TEM.^{1,20,22} We can compare our experimental results with the previous works, which facilitate our understanding of the Pt nanocrystal formation on MoS₂. The formation of Pt nanocrystals in MoS₂ liquid cells are observed by low-resolution *in situ* TEM imaging ([Figure S17 and Movie S1 in SI](#)) and energy dispersive X-ray spectroscopy ([Figure S18 in SI](#)). Most Pt nanocrystals are formed within a short period of the time (less than 10 sec). As the reaction proceeds, the growth of nanocrystals results in an increased image contrast. The Pt nanocrystals show narrow size distribution with an average diameter of ~2.5 nm (standard deviation of ~0.3 nm, [Figure S19 in SI](#)).

High-resolution *in situ* TEM images ([Figure 4a and Movie S2](#)) reveal the growth trajectories of individual ultra-small Pt nanocrystals (~2–3 nm) in MoS₂ liquid cells, showing representative of two populations of nanocrystals. One nanocrystal (marked as NC1) appears within ~10 sec and the other nanocrystal (marked as NC2) is formed much later after ~50 sec.

This is different from the previous observations that most nanocrystals are formed concurrently with a burst nucleation.^{90,91} Additional high-resolution *in situ* TEM data also show the consistent results (Figures S20, S21 and Movie S3 in SI) that there are two populations of Pt nanocrystals corresponding to the different formation time. In addition, the translational and rotational motions of Pt nanocrystals are suppressed during growth (Figure 4b), which is in contrast with the previous observations that small Pt nanocrystals (~2–3 nm) actively move and rotate in graphene liquid cells (Figure S22 and Movie S4 in SI) under the similar experimental conditions (i.e. with the similar solvent and electron beam intensity).^{20,22} This implies that the MoS₂ sheets play a role on Pt nanocrystal formation, which will be discussed further in below.

The FFT image of the first frame image (t_0) of Figure 4a exhibits hexagonally arranged spots corresponding to MoS₂ {100} lattice spacing (Figure 4c). Pt nanocrystals are absent at the initial stage. Pt nanocrystals appear as the reaction proceeds, which is confirmed by high resolution TEM imaging (Figure 4a) and the emergent of additional spots in FFT patterns (marked with white circles in Figure 4d,e). The observed lattice fringes for NC1 and NC2 are corresponding to Pt (111) and Pt (002) planes, respectively. The measured lattice parameters (Pt(111): 2.30 Å and Pt (200): 1.95 Å) are similar to those of the bulk crystals (Pt(111): 2.265 Å and Pt(200): 1.96 Å). Strikingly, the Pt (111) plane of NC1 are aligned with the MoS₂ {100} plane with slight misorientation (< 5°) (Figure 4f), while there is no obvious relationship between Pt (002) and MoS₂ {100}. We further analyze more Pt nanocrystals and find that the (111) and (002) lattice planes are prominent among the Pt nanocrystals formed inside the MoS₂ liquid cells. We measure the relative crystal orientation of Pt {111} and Pt {002} lattice planes to MoS₂ {100} planes (Figure 4g and Figure S23, S24 in SI). The results show that a large fraction of Pt nanocrystals are aligned with MoS₂ with the relationship of Pt {111} // MoS₂ {100}, while there is no obvious alignment between Pt {002} and MoS₂ (Figure 4h), which are

consistent with the above observation. Additional high-resolution *in situ* TEM images are obtained showing the orientation relationship of Pt (111)//MoS₂ {100} (Figures S20, S21 and Movie S3). The alignment between Pt (111) and MoS₂ {100} can be explained by the van der Waals epitaxy, which may reduce the formation energy of MoS₂-Pt heterostructures. Our results are consistent with the previous studies on solution-phase synthesis of Pt nanocrystals on MoS₂, where co-existence of both epitaxially aligned and randomly oriented Pt nanocrystals were observed.^{54,56} Interestingly, the two different growth trajectories of Pt nanocrystals observed in the above are correlated with the epitaxial relationship between Pt nanocrystals and MoS₂ substrate. Pt nanocrystals that are epitaxial with MoS₂ (NC1 in Figure 4a and NC3 in Figure S20 in SI) are formed earlier than those with random orientation (NC2 in Figure 4a and NC4 in Figure S20 in SI). This suggests the reduced energy barrier for heterogeneous nucleation of Pt nanocrystals on MoS₂ and the van der Waals epitaxy between MoS₂ and Pt nanocrystals may stabilize the heterostructures^{40-46,54,56,92,93}.

In summary, we have developed the efficient polymer-free MoS₂ transfer method and have showcased the MoS₂ liquid cell electron microscopy study of Pt nanocrystal formation on MoS₂. The polymer-free MoS₂ transfer is achieved by the selective etching of the interfacial SiO₂ layer of the substrate. Finite element analysis supports that our polymer-free transfer method can greatly reduce the mechanical damage leading to high transfer yield. The resulting clean MoS₂ surface is significant for fundamental studies and various applications. Our liquid cell TEM study of Pt nanocrystal formation on MoS₂ shows that the (111) plane of Pt nanocrystals has the strong tendency to align with the (001) plane of MoS₂, suggesting the van der Waals epitaxial relationship between Pt nanocrystals and the supporting MoS₂ sheets. Our study offers a new prototype to reveal nanocrystal formation on 2D materials and provides an effective method for polymer-free transfer of MoS₂, which is potentially applicable in a wide range of studies.

ASSOCIATED CONTENT

Supporting Information

The Supporting Information is available free of charge on the ACS Publications website at DOI:

Experimental methods, schematic illustrations, SEM images, FEM simulation results, and additional TEM analysis data (PDF)

In situ TEM Movie S1–S4 (AVI)

AUTHOR INFORMATION

Corresponding Authors

*E-mail: hmzheng@lbl.gov (H.Z.)

Author Contributions

J.Y. and M.K.C. contributed equally to this work.

Notes

The authors declare no competing financial interest.

ACKNOWLEDGMENT

This work was supported by the U.S. Department of Energy, Office of Science, Office of Basic Energy Sciences, Materials Sciences and Engineering Division, under Contract No. DE-AC02-05CH11231 within the insitu TEM program (KC22ZH). Work at the Molecular Foundry was supported by the Office of Science, Office of Basic Energy Sciences, of the U.S. Department of Energy under Contract No. DE-AC02-05CH11231.

References

- (1) Zheng, H.; Smith, R. K.; Jun, Y.-w.; Kisielowski, C.; Dahmen, U.; Alivisatos, A. P. *Science* **2009**, *324*, 1309–1312.
- (2) Nielsen, M. H.; Aloni, S.; De Yoreo, J.J. *Science* **2014**, *345*, 1158–1162.
- (3) Woehl, T. J.; Evans, J. E.; Arslan, I.; Ristenpart, W. D.; Browning, N. D. *ACS Nano* **2012**, *6*, 8599–8610.
- (4) De Yoreo, J. J.; Sommerdijk N. A. J. M. *Nat. Rev. Mater.* **2016**, *1*, 16035.
- (5) Sutter, P.; Li, Y.; Argyropoulos, C.; Sutter, E. *J. Am. Chem. Soc.* **2017**, *139*, 6771–6776.
- (6) Hauwiller, M. R.; Zhang, X.; Liang, W.-I.; Chiu, C.-H.; Zhang, Q.; Zheng, W.; Ophus, C.; Chan, E. M.; Czarnik, C.; Pan, M.; Ross, F. M.; Wu, W.-W.; Chu, Y.-H.; Asta, M.; Voorhees, P. W.; Alivisatos, A. P.; Zheng, H. *Nano Lett.* **2018**, *18*, 6427–6433.
- (7) Liao, H.-G.; Zhrebetskyy, D.; Xin, H.; Czarnik, C.; Ercius, P.; Elmlund, H.; Pan, M.; Wang, L.-W.; Zheng, H. *Science* **2014**, *345*, 916–919.
- (8) Sutter, E.; Jungjohann, K.; Bliznakov, S.; Courty, A.; Maisonhaute, E.; Tenney, S.; Sutter, P. *Nat. Commun.* **2014**, *5*, 4946.
- (9) Gao, W.; Hou, Y.; Hood, Z. D.; Wang, X.; More, K.; Wu, R.; Xia, Y.; Pan, X.; Chi, M. *Nano Lett.* **2018**, *18*, 7004–7013.
- (10) Kim, B. H.; Yang, J.; Lee, D.; Choi, B. K.; Hyeon, T.; Park, J. *Adv. Mater.* **2018**, *30*, 1703316.
- (11) Powers, A. S.; Liao, H.-G.; Raja, S. N.; Bronstein, N. D.; Alivisatos, A.P.; Zheng, H. *Nano Lett.* **2016**, *17*, 15–20.
- (12) Lee, W. C.; Kim, B. H.; Choi, S.; Takeuchi, S.; Park, J. *J. Phys. Chem. Lett.* **2017**, *8*, 647–654.
- (13) Tan, S. F.; Chee, S. W.; Lin, G.; Mirsaidov, U. *Acc. Chem. Res.* **2017**, *50*, 1303–1312.

- (14) Luo, B.; Smith, J. W.; Ou, Z.; Chen, Q. *Acc. Chem. Res.* **2017**, *50*, 1125–1133.
- (15) Williamson, M. J.; Tromp, R. M.; Vereecken, P. M.; Hull, R.; Ross, F. M. *Nat. Mater.* **2003**, *2*, 532–536.
- (16) Gu, M.; Parent, L. R.; Mehdi, B. L.; Unocic, R. R.; McDowell, M. T.; Sacci, R. L.; Xu, W.; Connell, J. G.; Xu, P.; Abellan, P.; Chen, X.; Zhang, Y.; Perea, D. E.; Evans, J. E.; Lauhon, L. J.; Zhang, J.-G.; Liu, J.; Browning, N. D.; Cui, Y.; Arslan, I.; Wang, C.-M. *Nano Lett.* **2013**, *13*, 6106–6112.
- (17) Zeng, Z.; Zheng, W.; Zheng, H. *Acc. Chem. Res.* **2017**, *50*, 1808–1807.
- (18) Park, J.; Park, H.; Ercius, P.; Pegoraro, A. F.; Xu, C.; Kim, J. W.; Han, S. H.; Weitz, D. A.; *Nano Lett.* **2015**, *15*, 4737–4744.
- (19) Liv, N.; van Oosten Slingeland, D. S.; Baudoin, J. P.; Kruit, P.; Piston, D. W.; Hoogenboom, J. P. *ACS Nano* **2016**, *10*, 265–273.
- (20) Yuk, J. M.; Park, J.; Ercius, P.; Kim, K.; Hellebusch, D. J.; Crommie, M. F.; Lee, J. Y.; Zettl, A.; Alivisatos, A. P. *Science* **2012**, *336*, 61–64.
- (21) Chen, Q.; Smith, J. M.; Park, J.; Kim, K.; Ho, D.; Rasool, H. I.; Zettl, A.; Alivisatos, A. P. *Nano Lett.* **2013**, *13*, 4556–4561.
- (22) Park, J.; Elmlund, H.; Ercius, P.; Yuk, J. M.; Limmer, D. T.; Chen, Q.; Kim, K.; Han, S. H.; Weitz, D. A.; Zettl, A.; Alivisatos, A. P. *Science* **2015**, *349*, 290–295.
- (23) Ye, X.; Jones, M. R.; Frechette, L. B.; Chen, Q.; Powers, A. S.; Ercius, P.; Dunn, G.; Rotskoff, G. M.; Nguyen, S. C.; Adiga, V. P.; Zettl, A.; Rabani, E.; Geissler, P. L.; Alivisatos, A. P. *Science* **2016**, *354*, 874–877.
- (24) Dahmke, I. N.; Verch, A.; Hermannsdorfer, J.; Peckys, D. B.; Weatherup, R. S.; Hofmann, S.; de Jonge, N. *ACS Nano* **2017**, *11*, 11108–11117.
- (25) Nagamanasa, K. H.; Wang, H.; Granick, S. *Adv. Mater.* **2017**, *29*, 1703555.
- (26) Kelly, D.; Zhou, M.; Clark, N.; Hamer, M. J.; Lewis, E. A.; Rakowski, A. M.; Haigh, S.

- J.; Gorbachev, R. V. *Nano Lett.* **2018**, *18*, 1168–1174.
- (27) Textor, M.; de Jonge, N. *Nano Lett.* **2018**, *18*, 3313–3321.
- (28) de Jonge, N. *Ultramicroscopy* **2018**, *187*, 113–125.
- (29) Meyer, J. C.; Girit, C. O.; Crommie, M. F.; Zettl, A. *Nature* **2008**, *454*, 319–322.
- (30) Nair, R. R.; Blake, P.; Blake, J. R.; Zan, R.; Anissimova, S.; Bangert, U.; Golovanov, A. P.; Morozov, S. V.; Geim, A. K.; Novoselov, K. S.; Latychevskaya, T. *Appl. Phys. Lett.* **2010**, *97*, 153102.
- (31) Bolotin, K. I.; Sikes, K. J.; Jiang, Z.; Klima, M.; Fudenberg, G.; Hone, J.; Kim, P.; Stormer, H. L. *Solid State Commun.* **2008**, *146*, 351–355.
- (32) Aliofkhazraei, M.; Ali, N.; Milne, W. I.; Ozkan, C. S.; Mitura, S.; Gervasoni, J. L. *Graphene science handbook: electrical and optical properties*; CRC Press: Boca Raton, FL, **2016**.
- (33) Xu, K.; Cao, P.; Heath, J. R. *Science* **2010**, *329*, 1188–1191.
- (34) Lee, C.; Wei, X.; Kysar, J. W.; Hone, J. *Science* **2008**, *321*, 385–388.
- (35) Cho, H.; Jones, M. R.; Nguyen, S. C.; Hauwiller, M. R.; Zettl, A.; Alivisatos, A. P. *Nano Lett.* **2017**, *17*, 414–420.
- (36) Wang, H.; Nagamanasa, K. H.; Kim, Y.-J.; Kwon, O.-H.; Granick, S. *ACS Nano* **2018**, *12*, 8572–8578.
- (37) Yang, J.; Alam, S. B.; Yu, L.; Chan, E.; Zheng, H. *Micron* **2019**, *116*, 22–29.
- (38) Keskin, S.; de Jonge, N. *Nano Lett.* **2018**, DOI: 10.1021/acs.nanolett.8b02490
- (39) Krueger, M.; Berg, S.; Stone, D.; Strelcov, E.; Dikin, D. A.; Kim, J.; Cote, L. J.; Huang, J.; Kolmakov, A. *ACS Nano* **2011**, *5*, 10047–10057.
- (40) Huang, X.; Qi, X.; Boey, F.; Zhang, H. *Chem. Soc. Rev.* **2012**, *41*, 666–686.
- (41) Butler, S. Z.; Hollen, S. M.; Cao, L.; Cui, Y.; Gupta, J. A.; Gutiérrez, H. R.; Heinz, T. F.; Hong, S. S.; Huang, J.; Ismach, A. F.; Johnston-Halperin, E.; Kuno, M.; Plashnitsa,

- V. V.; Robinson, R. D.; Ruoff, R. S.; Salahuddin, S.; Shan, J.; Shi, L.; Spencer, M. G.; Terrones, M.; Windl, W.; Goldberger, J. E. *ACS Nano* **2013**, *7*, 2898–2926.
- (42) Geim, A. K.; Grigorieva, I. V. *Nature* **2013**, *499*, 419–425.
- (43) Yu, J. H.; Lee, H. R.; Hong, S. S.; Kong, D.; Lee, H.-W.; Wang, H.; Xiong, F.; Wang, S.; Cui, Y. *Nano Lett.* **2015**, *15*, 1031–1035.
- (44) Ban, H. W.; Park, S.; Jeong, H.; Gu, D. H.; Jo, S.; Park, S. H.; Park, J.; Son, J. S. *J. Phys. Chem. Lett.* **2016**, *7*, 3627–3635.
- (45) Liu, Y.; Weiss, N. O.; Duan, X.; Cheng, H.-C.; Huang, Y.; Duan, X. *Nat. Rev. Mater.* **2016**, *1*, 16042.
- (46) Yang, J.; Kim, K.; Lee, Y.; Kim, K.; Lee, W. C.; Park, J. *FlatChem* **2017**, *5*, 50–68.
- (47) Shi, J.; Ma, D.; Han, G.-F.; Zhang, Y.; Ji, Q.; Gao, T.; Sun, J.; Song, X.; Li, C.; Zhang, Y.; Liu, Z. *ACS Nano* **2014**, *8*, 10196–10204.
- (48) Deng, J.; Li, H.; Xiao, J.; Tu, Y.; Deng, D.; Yang, H.; Tian, H.; Li, J.; Ren, P.; Bao, X. *Energy Environ. Sci.* **2015**, *8*, 1594–1601.
- (49) Deng, D.; Novoselov, K. S.; Fu, Q.; Zheng, N.; Tian, Z.; Bao, X. *Nat. Nanotechnol.* **2016**, *11*, 218–230.
- (50) Li, H.; Wang, L.; Dai, Y.; Pu, Z.; Lao, Z.; Chen, Y.; Wang, M.; Zheng, X.; Zhu, J.; Zhang, W.; Si, R.; Ma, C.; Zeng, J. *Nat. Nanotechnol.* **2018**, *13*, 411–417.
- (51) Li, Y.; Majewski, M. B.; Islam, S. M.; Hao, S.; Murthy, A. A.; DiStefano, J. G.; Hanson, E. D.; Xu, Y.; Wolverton, C.; Kanatzidis, M. G.; Wasielewski, M. R.; Chen, X.; Dravid, V. P. *Nano Lett.* **2018**, *18*, 7104–7110.
- (52) Zhang, Y.; Tang, T.-T.; Girit, C.; Hao, Z.; Martin, M. C.; Zettl, A.; Crommie, M. F.; Shen, Y. R.; Wang, F. *Nature* **2009**, *459*, 820–823.

- (53) Yankowitz, M.; Xue, J.; Cormode, D.; Sanchez-Yamagishi, J. D.; Watanabe, K.; Taniguchi, T.; Jarillo-Herrero, P.; Jacquod, P.; LeRoy, B. J. *Nat. Phys.* **2012**, *8*, 382–386.
- (54) Huang, X.; Zeng, Z.; Bao, S.; Wang, M.; Qi, X.; Fan, Z.; Zhang, H. *Nat. Commun.* **2013**, *4*, 1444.
- (55) Li, H.; Wang, S.; Sawada, H.; Han, G. G. D.; Samuels, T.; Allen, C. S.; Kirkland, A. I.; Grossman, J. C.; Warner, J. H. *ACS Nano* **2017**, *11*, 3392–3403.
- (56) Wang, S.; Sawada, H.; Chen, Q.; Han, G. G. D.; Allen, C.; Kirkland, A. I.; Warner, J. H. *ACS Nano* **2017**, *11*, 9057–9067.
- (57) Kim, K. S.; Zhao, Y.; Jang, H.; Lee, S. Y.; Kim, J. M.; Kim, K. S.; Ahn, J.-H.; Kim, P.; Choi, J.-Y.; Hong, B. H. *Nature* **2009**, *457*, 706–710.
- (58) Li, H.; Wu, J.; Huang, X.; Yin, Z.; Liu, J.; Zhang, H. *ACS Nano* **2014**, *8*, 6563–6570.
- (59) Akinwande, D.; Petrone, N.; Hone, J. *Nat. Commun.* **2014**, *5*, 5678.
- (60) Chang, H.-Y.; Yang, S.; Lee, J.; Tao, L.; Hwang, W.-S.; Jena, D.; Lu, N.; Akinwande, D. *ACS Nano* **2013**, *7*, 5446–5452.
- (61) Choi, C.; Choi, M. K.; Liu, S.; Kim, M. S.; Park, O. K.; Kim, J.; Kim, C.; Qin, X.; Lee, G. J.; Cho, K. W.; Kim, M.; Joh, E.; Lee, J.; Son, D.; Kwon, S.-H.; Jeon, N. L.; Song, Y. M.; Lu, N.; Kim, D.-H. *Nat. Commun.* **2017**, *8*, 1664.
- (62) Hong, X.; Kim, J.; Shi, S.-F.; Zhang, Y.; Jin, C.; Sun, Y.; Tongay, S.; Wu, J.; Zhang, Y.; Wang, F.; *Nat. Nanotechnol.* **2014**, *9*, 682–686.
- (63) Schmidt, H.; Wang, S.; Chu, L.; Toh, M.; Kumar, R.; Zhao, W.; Neto, A. H. C.; Martin, J.; Adam, S.; Özyilmaz, B.; Eda, G. *Nano Lett.* **2014**, *14*, 1909–1913.
- (64) Zhan, Y.; Liu, Z.; Najmaei, S.; Ajayan, P. M.; Lou, J. arXiv:1111.5072.
- (65) Zhang, Z.; Du, J.; Zhang, D.; Sun, H.; Yin, L.; Ma, L.; Chen, J.; Ma, D.; Cheng, H.-M.; Ren, W. *Nat. Commun.* **2017**, *8*, 14560.

- (66) Suk, J. W.; Kitt, A.; Magnuson, C. W.; Hao, Y.; Ahmed, S.; An, J.; Swan, A. K.; Goldberg, B. B.; Ruoff, R. S. *ACS Nano* **2011**, *5*, 6916–6924.
- (67) Lock, E. H.; Baraket, M.; Laskoski, M.; Mulvaney, S. P.; Lee, W. K.; Sheehan, P. E.; Hines, D. R.; Robinson, J. T.; Tosado, J.; Fuhrer, M. S.; Hernandez, S. C.; Walton, S. G. *Nano Lett.* **2012**, *12*, 102–107.
- (68) Song, J.; Kam, F.-Y.; Png, R.-Q.; Seah, W.-L.; Zhuo, J.-M.; Lim, G.-K.; Ho, P. K. H.; Chua, L.-L. *Nat. Nanotechnol.* **2013**, *8*, 356–362.
- (69) Gao, L.; Ni, G.-X.; Liu, Y.; Liu, B.; Neto, A. H. C.; Loh, K. P. *Nature* **2014**, *505*, 190–194.
- (70) Lin, Z.; Zhao, Y.; Zhou, C.; Zhong, R.; Wang, X.; Tsang, Y. H.; Chai, Y. *Sci. Rep.* **2015**, *5*, 18596.
- (71) Choi, M. K.; Park, I.; Kim, D. C.; Joh, E.; Park, O. K.; Kim, J.; Kim, M.; Choi, C.; Yang, J.; Cho, K. W.; Hwang, J.-H.; Nam, J.-M.; Hyeon, T.; Kim, J. H.; Kim, D.-H. *Adv. Funct. Mater.* **2015**, *25*, 7109–7118.
- (72) Bae, S.; Kim, H.; Lee, Y.; Xu, X.; Park, J.-S.; Zheng, Y.; Balakrishnan, J.; Lei, T.; Kim, H. R.; Song, Y. I.; Kim, Y.-J.; Kim, K. S.; Ozyilmaz, B.; Ahn, J.-H.; Hong, B. H.; Iijima, S. *Nat. Nanotechnol.* **2010**, *5*, 574–578.
- (73) Wang, X.; Tao, L.; Hao, Y.; Liu, Z.; Chou, H.; Kholmanov, I.; Chen, S.; Tan, C.; Jayant, N.; Yu, Q.; Akinwande, D.; Ruoff, R. S. *Small* **2014**, *10*, 694–698.
- (74) Jung, W.; Kim, D.; Lee, M.; Kim, S.; Kim, J.-H.; Han, C.-S. *Adv. Mater.* **2014**, *26*, 6394–6400.
- (75) Abellan, P.; Woehl, T. J.; Parent, L. R.; Browning, N. D.; Evans, J. E.; Arslan, I. *Chem. Commun.* **2014**, *50*, 4873–4880.
- (76) Woehl, T. J.; Abellan, P. *J. Microsc.* **2017**, *265*, 135–147.
- (77) Regan, W.; Alem, N.; Alemán, B.; Geng, B.; Girit, C.-.; Maserati, L.; Wang, F.;

- Crommie, M.; Zettl, A. *Appl. Phys. Lett.* **2010**, *96*, 113102.
- (78) Lin, W.-H.; Chen, T.-H.; Chang, J.-K.; Taur, J.-I.; Lo, Y.-Y.; Lee, W.-L.; Chang, C.-S.; Su, W.-B.; Wu, C.-I. *ACS Nano* **2014**, *8*, 1784–1791.
- (79) Zhang, J.; Lin, L.; Sun, L.; Huang, Y.; Koh, A. L.; Dang, W.; Yin, J.; Wang, M.; Tan, C.; Li, T.; Tan, Z.; Liu, Z.; Peng, H. *Adv. Mater.* **2017**, *29*, 1700639.
- (80) Tsai, M.-L.; Su, S.-H.; Chang, J.-K.; Tsai, D.-S.; Chen, C.-H.; Wu, C.-I.; Li, L.-J.; Chen, L.-J.; He, J.-H. *ACS Nano* **2014**, *8*, 8317–8322.
- (81) Gurarslan, A.; Yu, Y.; Su, L.; Yu, Y.; Suarez, F.; Yao, S.; Zhu, Y.; Ozturk, M.; Zhang, Y.; Cao, L. *ACS Nano* **2014**, *8*, 11522–11528.
- (82) Yu, H.; Liao, M.; Zhao, W.; Liu, G.; Zhou, X. J.; Wei, Z.; Xu, X.; Liu, K.; Hu, Z.; Deng, K.; Zhou, S.; Shi, J.-A.; Gu, L.; Shen, C.; Zhang, T.; Du, L.; Xie, L.; Zhu, J.; Chen, W.; Yang, R.; Shi, D.; Zhang, G. *ACS Nano* **2017**, *11*, 12001–12007.
- (83) Ma, D.; Shi, J.; Ji, Q.; Chen, K.; Yin, J.; Lin, Y.; Zhang, Y.; Liu, M.; Feng, Q.; Song, X.; Guo, X.; Zhang, J.; Zhang, Y.; Liu, Z. *Nano Res.* **2015**, *8*, 3662–3672.
- (84) Lee, Y.-H.; Yu, L.; Wang, H.; Fang, W.; Ling, X.; Shi, Y.; Lin, C.-T.; Huang, J.-K.; Chang, M.-T.; Chang, C.-S.; Dresselhaus, M.; Palacios, T.; Li, L.-J.; King, J. *Nano Lett.* **2013**, *13*, 1852–1857.
- (85) Jimenez, S.; Sandoval, D.; Yang, D. Frindt, R. F.; Irwin, J. C. *Phys. Rev. B* **1991**, *44*, 3955–3962.
- (86) Li, H.; Zhang, Q.; Yap, C. C. R.; Tay, B. K.; Edwin, T. H. T.; Olivier, A.; Baillargeat D. *Adv. Funct. Mater.* **2012**, *22*, 1385–1390.
- (87) Zhang, X.; Qiao, X.-F.; Shi, W.; Wu, J.-B.; Jiang, D.-S.; Tan, P.-H. *Chem. Soc. Rev.* **2015**, *44*, 2757–2785.
- (88) Ferrari, A. C.; Meyer, J. C.; Scardaci, V.; Casiraghi, C.; Lazzeri, M.; Mauri, F.; Piscanec, S.; Jiang, D.; Novoselov, K. S.; Roth, S.; Geim, A. K. *Phys. Rev. Lett.* **2006**, *97*, 187401.

- (89) de Jonge, N.; Peckys, D. B.; Kremers, G. J.; Piston, D. W. *Proc. Natl. Acad. Sci USA* **2009**, *106*, 2159–2164.
- (90) Sugimoto, T. *Adv. Colloid Interfac. Sci.* **1987**, *28*, 65–108.
- (91) Kwon, S. G.; Hyeon, T. *Small* **2011**, *7*, 2685–2702.
- (92) Lee, W. C., Kim, K., Park, J., Koo, J., Jeong, H. Y., Lee, H., Weitz, D. A., Zettl, A., Takeuchi, S. *Nat. Nanotechnol.* **2015**, *10*, 423–428.
- (93) Jang, J.; Lee, Y.; Yoon, J.-Y.; Yoon, H. H.; Koo, J.; Choe, J.; Jeon, S.; Sung J.; Park, J.; Lee, W. C.; Lee, H.; Jeong, H. Y.; Park, K.; Kim. K. *Nano Lett.* **2018**, *18*, 6214–6221.

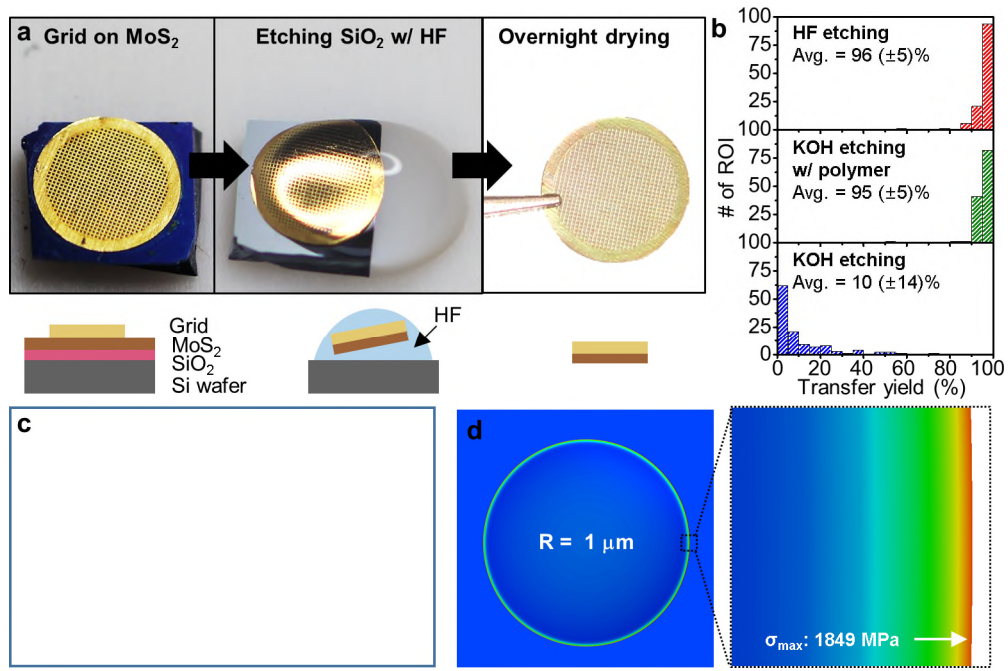


Figure 1. Polymer-free transfer process of MoS₂. (a) Optical images (top) and the corresponding cross-sectional schematics (bottom) showing the polymer-free transfer method. (b) Histograms showing the distribution of the transfer yield among the region of interest (ROI) according to the transfer methods. 120 ROIs with 100 holes were used for each histogram. (c,d) Finite element method simulation of the stress distribution on MoS₂ sheet by (c) bending and (d) stretching (bubble attachment).

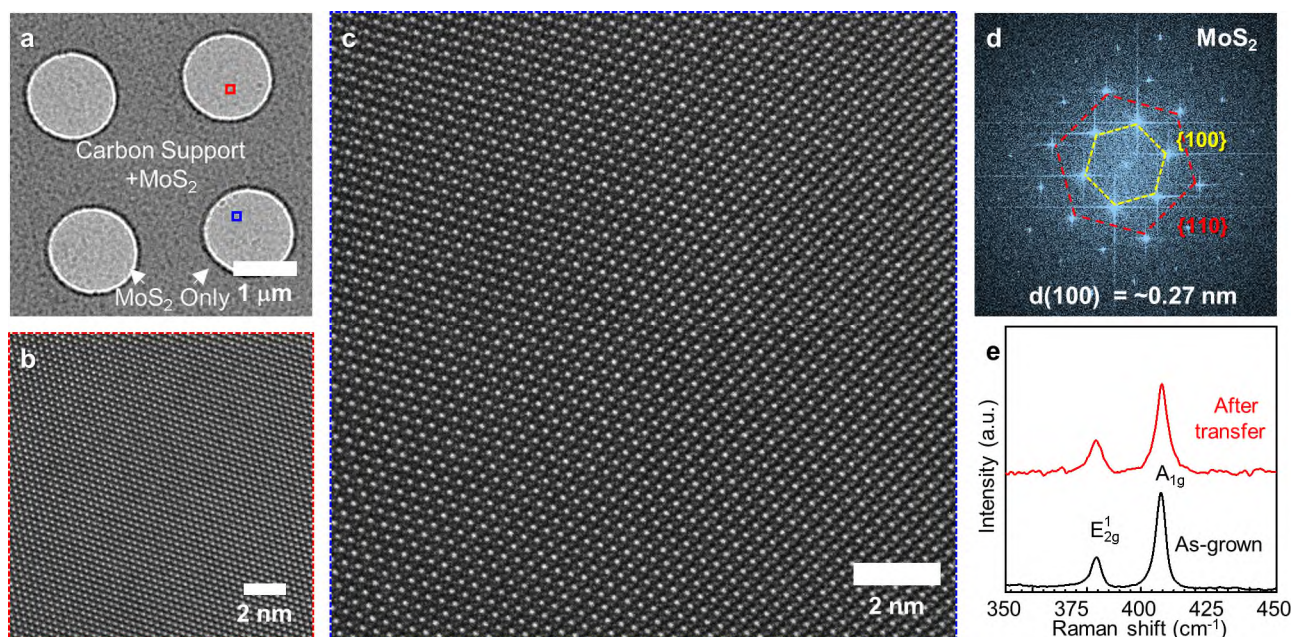


Figure 2. Characterization of polymer-free transferred MoS₂. (a) Low-resolution TEM image showing the overall configuration of MoS₂-transferred TEM grids. MoS₂ membrane is transferred on the holey carbon support with the hole size of ~1.2 μm. (b,c) Atomic-resolution TEM images of transferred MoS₂ and (d) the FFT image of the panel (c). Crystal orientation of MoS₂ in the panel (b) and (c) is slightly different, because of the polycrystalline nature of multilayer MoS₂. The images are obtained from boxed area of the panel (a). (e) Raman spectra of MoS₂ on SiO₂ (black) before the transfer process and MoS₂ TEM grids (red).

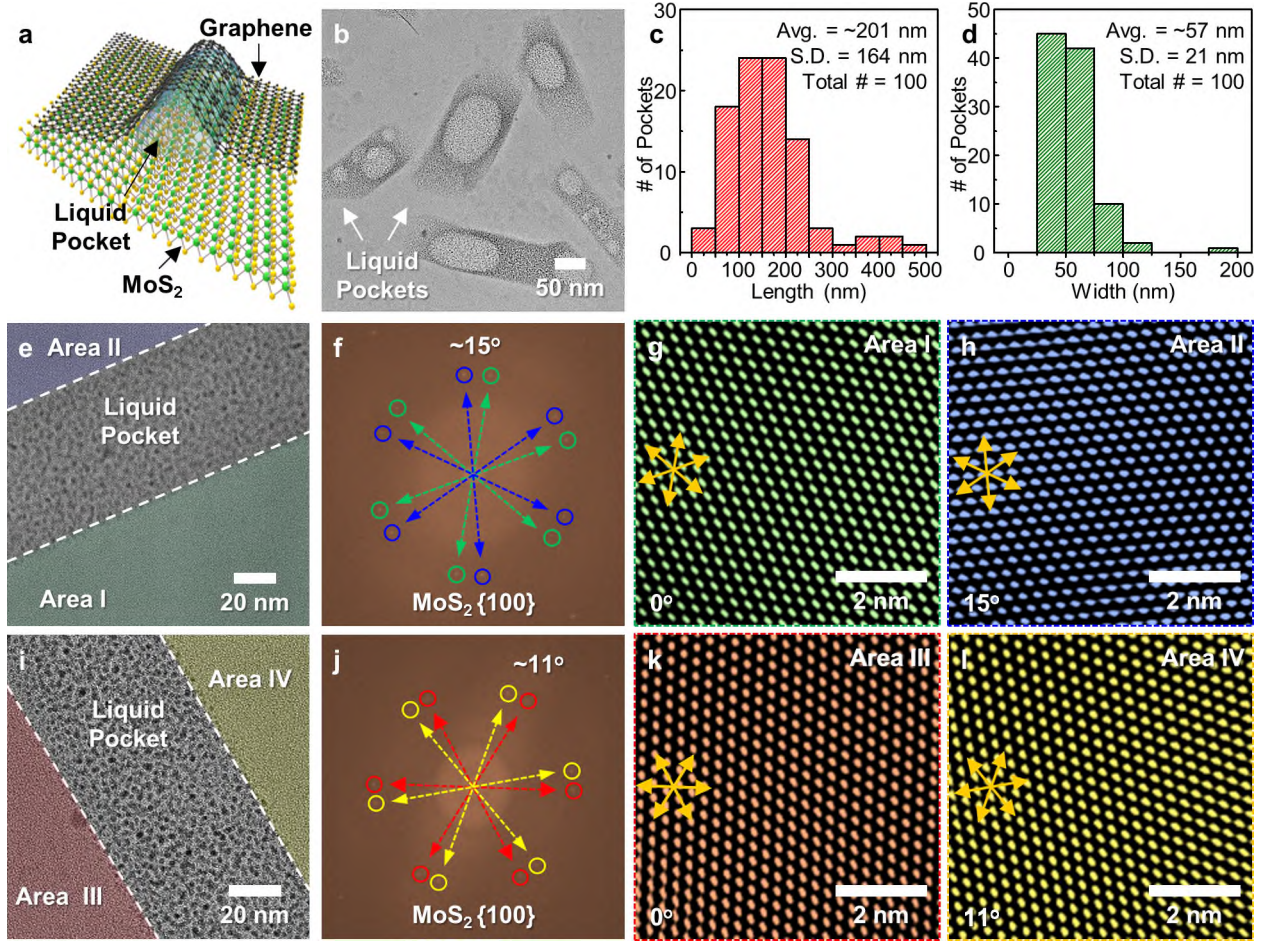


Figure 3. Liquid pocket formation in MoS₂ liquid cells. (a) Schematic illustration showing MoS₂ liquid cells. (b) Low-resolution TEM image showing the overall shape of liquid pockets formed in MoS₂ liquid cells. (c,d) Histograms showing the distribution of (c) the length and (d) width of liquid pockets. (e) TEM image of a liquid pocket with 4k×4k resolution and (f) the corresponding FFT. The areas with the different MoS₂ grains are highlighted by green (area I) and blue (area II). (g,h) Parts of high-resolution filtered-inverse FFT images for each area. The orange arrows indicate the MoS₂ <100> axes. Area I and area II are related to green and blue circled spots in the FFT image, respectively. (i) Another color-mapped TEM image showing the MoS₂ grain distribution and (j) the corresponding FFT. The areas with the different MoS₂ grains are highlighted by red (area III) and yellow (area IV). (k,l) Parts of high-resolution filtered-inverse FFT images for each area. The orange arrows indicate the MoS₂ <100> axes. Area III and area IV are related to red and yellow circled spots in the FFT image, respectively.

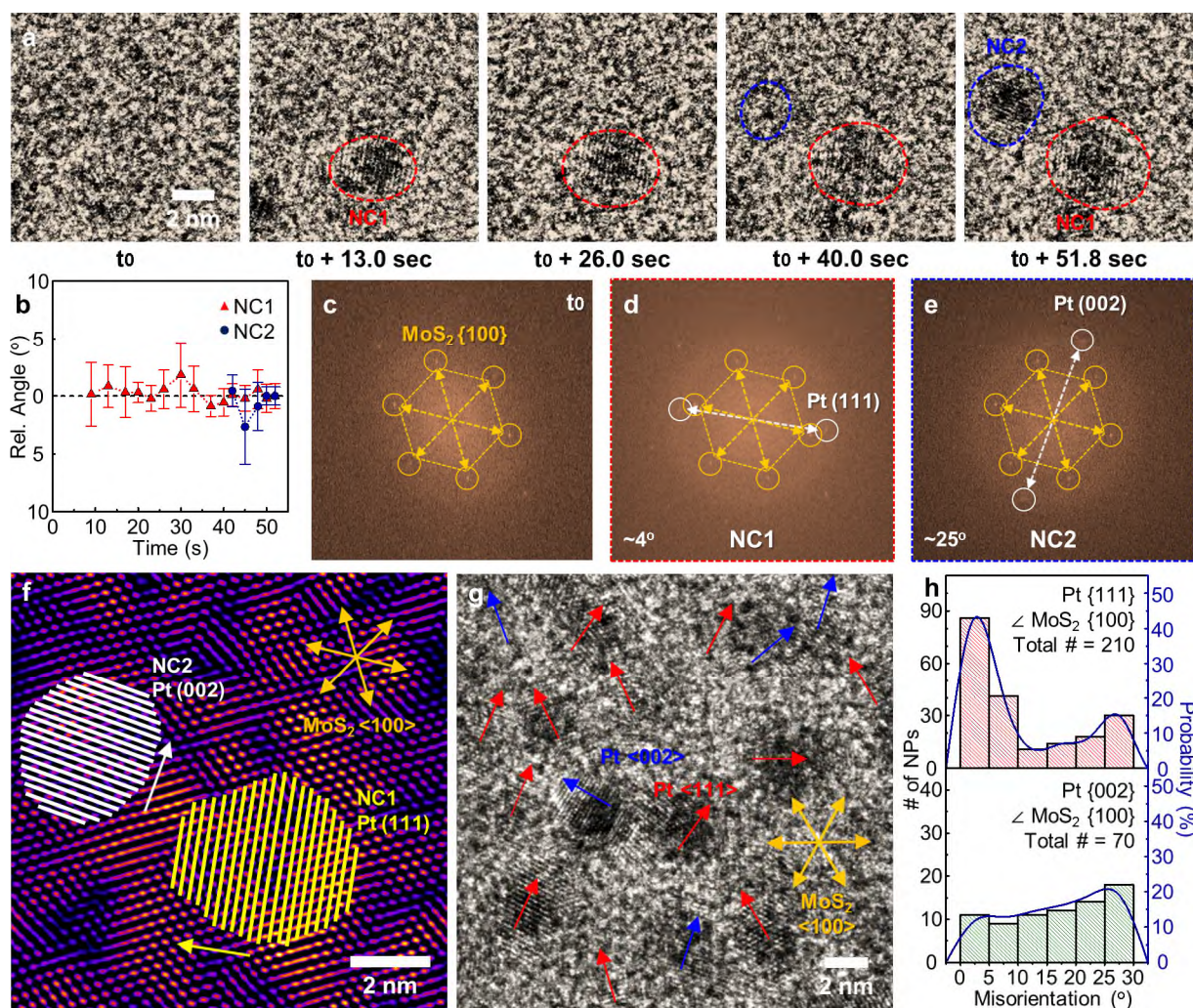


Figure 4. Formation of Pt nanocrystals on MoS₂. (a) A time-series of high-resolution *in situ* TEM images showing the formation of individual Pt nanocrystals. The corresponding movie is displayed in [Movie S2](#). (b) A plot showing the relative orientation Pt nanocrystals of as a function of the time. The orientation at the last time frame is set as 0° for the both nanocrystals. (c–e) FFT of the first image (t_0) and formed Pt nanocrystals. (f) Atomic level image based on inverse FFT of the last time frame image ($t_0 + 51.8$ sec) of the panel (a), showing the relative crystalline orientation of Pt nanocrystals and MoS₂. (g) TEM image showing the orientation of the Pt nanocrystals. The orientation of Pt <111> and Pt <002> are marked with blue and red arrows, respectively. MoS₂ <100> direction is indicated by the orange arrows. (h) Histograms showing the misalignment angle between the lattice planes of Pt nanocrystals (Pt {111} and Pt {002}) and MoS₂ {100} plane. The data are acquired from 210 nanocrystals for {111} and 70 nanocrystals for {002}. The blue solid lines indicate the probability

Table of Contents Graphic

